# Measurement of the long-lived $^{26}$Al production cross section in the $^{27}$Al($n$,$2n$) reaction

T. Nakamura and H. Sugita
*Cyclotron and Radioisotope Center, Tohoku University, Aoba, Aramaki, Sendai 980, Japan*

M. Imamura and Y. Uwamino
*Institute for Nuclear Study, University of Tokyo, Midori-cho 3-2-1, Tanashi, Tokyo 188, Japan*

H. Nagai
*College of Humanities and Sciences, Nihon University, Sakura-Johsui, Setagaya, Tokyo 156, Japan*

K. Kobayashi
*Research Center for Nuclear Science and Technology, University of Tokyo, Yayoi 2-11-16, Bunkyo, Tokyo 113, Japan*
(Received 13 August 1990)

Experimental data for the $^{27}$Al($n$,$2n$)$^{26}$Al cross section have never been reported in the neutron energy range above 15 MeV, since the detection of the long-lived $^{26}$Al (half-life of $7.2\times10^5$ yr) necessitates an intense high-energy neutron source and highly sensitive detection method. We have measured the $^{27}$Al($n$,$2n$)$^{26}$Al cross section in the energy range of 14–36 MeV by using a semimonoenergetic neutron beam from the Be($p$,$n$) reaction. The activity of $^{26}$Al was measured by the accelerator mass spectrometry method and we found that the cross section has a maximum value of 95 mb in the neutron energy range of 20–24 MeV.

## I. INTRODUCTION

Aluminum is now being suggested as a material for accelerator tubes and fusion plasma vessels because of its lower and faster-decaying residual radioactivity when compared to stainless steel or copper, which have been commonly used. For long-term operation of these machines, however, the accumulation of long-lived $^{26}$Al (spin of $5^+$, half-life of $7.2\times10^5$ yr) produced by the $^{27}$Al($n$,$2n$) reaction in an intense neutron field may be a serious problem.

As for the $^{27}$Al($n$,$2n$)$^{26}$Al cross section, several measurements have been published[1–3] in the neutron energy range around 14 MeV. These cross-section data were obtained from the direct measurement of 1.809 MeV gamma rays followed the beta decay of $^{26}$Al and also from the accelerator mass spectrometry (AMS), which has been pioneered at Argonne.[4] This measurement required the intense neutron beam irradiation in order to produce enough $^{26}$Al activity for gamma-ray counting. But no experimental data on this cross section above 15 MeV have ever been published because of the lack of monoenergetic neutron sources of high intensity.

Here in this study, we have measured the $^{27}$Al($n$,$2n$)$^{26}$Al cross section in the energy range of 14–40 MeV by using a semimonoenergetic neutron beam settled at the SF cyclotron of the Institute for Nuclear Study, University of Tokyo.[5] In this experiment, we have measured the $^{26}$Al activity by the AMS system using the internal beam-monitor method[6] at the tandem Van de Graaf accelerator of the Research Center for Nuclear Science and Technology, University of Tokyo, which has been equipped for this method. This highly effective method made it possible to detect the $^{26}$Al activity after the short-period neutron irradiation.

## II. NEUTRON IRRADIATION EXPERIMENT

A proton beam of energies of 20, 22.5, 25, 27.5, 30, 32.5, 35, 37.5, and 40 MeV is extracted from the cyclotron and hits the 1-mm-thick ($E_p$=20–37.5 MeV) and 2-mm-thick ($E_p$=40 MeV) Be targets which are backed by the water coolant. The proton beam partially loses its energy in the Be target and fully stops in the water. The water is simultaneously used to absorb the residual proton energy because of the small neutron production cross section of $^{16}$O($p$,$n$). The target system was electrically insulated from the surroundings and the beam current incident to the target was measured with a current integrator. The energy loss of protons in the target is shown in Table I.

The neutron spectra at 0° were measured with a 51-mm-diameter by 51-mm-long NE-213 scintillator placed 1.3 m from the Be target. A $n$-$\gamma$ discrimination technique was utilized and the pulse-height distribution by neutrons was unfolded to an energy spectrum with the revised FERDO code[7] and the response function matrix.[8] With the same detector system, the room-scattered neutron flux was also measured by placing a concrete shadow bar of 10 cm by 10 cm by 50 cm long, which shielded the direct neutrons from the target.

Since the neutron spectrum measurement has been described in other papers by Uwamino *et al.*,[5,9] a brief description on final results is presented in this report. The measured neutron spectra which subtracted the room-scattered components are shown with the unfolded errors in Fig. 1. In the figure, the monoenergetic peak neutron energy is indicated for each proton energy, and the former is 4 to 5 MeV lower than the latter. The characteristics of neutron spectra are shown in Table I.

The aluminum samples (MARZ grade, 5×5 mm in

 

TABLE I. Characteristics of semimonoenergetic *p*-Be neutron field.

| Proton energy (MeV) | 40.0 | 37.5 | 35.0 | 32.5 | 30.0 | 27.5 | 25.0 | 22.5 | 20.0 |
|---|---|---|---|---|---|---|---|---|---|
| Target thickness (mm) | 2.0 | 1.0 | 1.0 | 1.0 | 1.0 | 1.0 | 1.0 | 1.0 | 1.0 |
| Proton energy loss in Be target (MeV) | 4.73 | 2.44 | 2.59 | 2.76 | 2.96 | 3.21 | 3.50 | 3.87 | 4.35 |
| Total neutron yield above 4.0 MeV (neutron $sr^{-1} C^{-1}$) | $1.60\times10^{16}$ | $7.72\times10^{15}$ | $6.16\times10^{15}$ | $6.76\times10^{15}$ | $6.28\times10^{15}$ | $5.48\times10^{15}$ | $4.80\times10^{15}$ | $4.32\times10^{15}$ | $3.72\times10^{15}$ |
| Peak region (MeV) | 30.0–39.0 | 30.0–36.0 | 28.0–34.0 | 25.0–31.0 | 22.0–29.0 | 19.0–26.0 | 17.0–24.0 | 14.0–21.0 | 11.0–19.0 |
| Average peak energy (MeV) | 35.0 | 33.6 | 31.2 | 28.5 | 25.9 | 23.4 | 21.0 | 18.2 | 15.3 |
| Peak neutron yield (neutron $sr^{-1}C^{-1}$) | $7.46\times10^{15}$ | $3.03\times10^{15}$ | $2.41\times10^{15}$ | $3.24\times10^{15}$ | $3.29\times10^{15}$ | $2.86\times10^{15}$ | $2.24\times10^{15}$ | $2.22\times10^{15}$ | $1.99\times10^{15}$ |
| Percentage of peak area | 46.5 | 39.3 | 39.1 | 47.9 | 52.4 | 52.2 | 46.6 | 51.5 | 53.4 |

size and 50 $\mu$m thickness and the purity is 99.999%) were irradiated at two positions of 5 and 10 cm from the Be target for about 15 h. The proton beam current for neutron irradiation was 3 to 5 $\mu$A and was kept as constant as possible during the irradiation. The irradiation to aluminum samples was carried out for seven proton energies of $E_p = 20.0$, 22.5, 25.0, 27.5, 30.0, 32.5, and 37.5 MeV.

## III. ACCELERATOR MASS SPECTROMETRY OF $^{26}$Al ACTIVITY

The measurement of $^{26}$Al produced by the $^{27}$Al$(n,2n)$ reaction was done by using accelerator mass spectrometry (AMS) system at the tandem Van de Graaf accelerator of the University of Tokyo which has been equipped for this method.

### A. AMS sample preparation

The aluminum samples were dissolved in HCl to get aluminum chloride by heating by an infrared lamp for 2–3 h. From the dried aluminum chloride, aluminum hydroxide was precipitated with ammonia water and separated from the solution by centrifuging. This precipitated $Al(OH)_3$ was redissolved in HCl with enriched $^{10}$B (91.8%) in the form of a boric acid solution. The added $^{10}$B amount was 2–3 $\mu$g/mg Al. The recovery of Al in this chemical procedure was almost 100%.

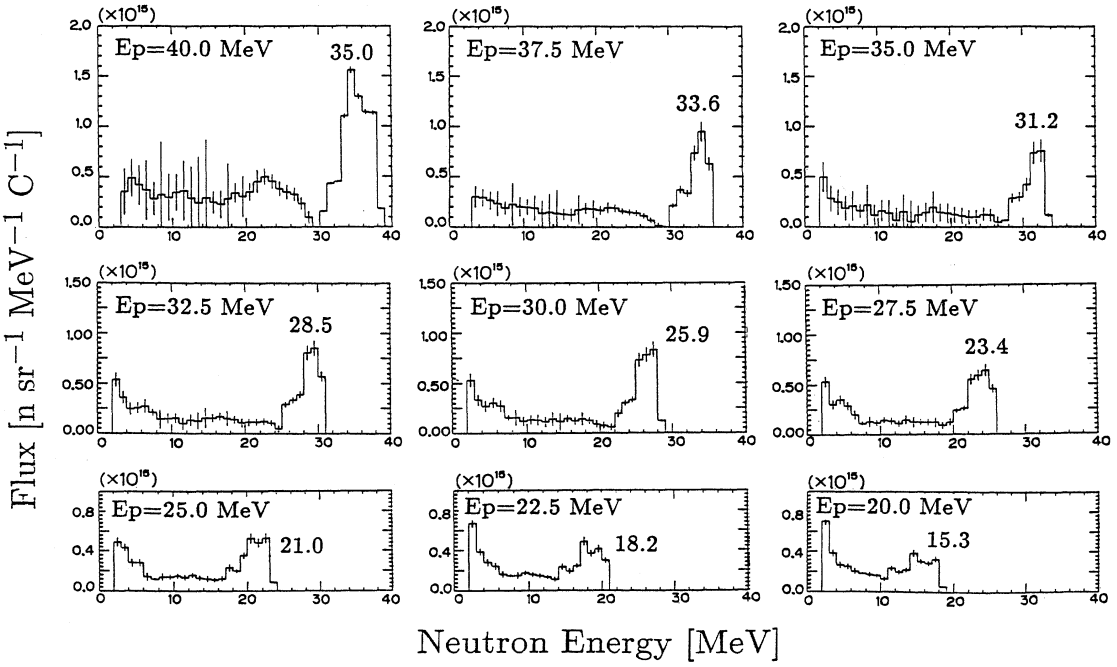


FIG. 1. Semimonoenergetic neutron energy spectra for proton energies of 20, 22.5, 25, 27.5, 30, 32.5, 35, 37.5, and 40 MeV.

This solution was put into a small quartz beaker and heated by an infrared lamp until nearly dry and further heated in an electric furnace at about 550 °C for 15–30 min to convert to $Al_2O_3$-$B_2O_3$ form. This $Al_2O_3$-$B_2O_3$ mixture was mixed well with Ag powder (100 mesh) and compressed into a 1.5-mm-diameter hole of a copper target cone of a Cs sputtering ion source.

### B. $^{26}$Al/$^{27}$Al isotopic ratio

Figure 2 shows a schematic of a beam-monitor method for $^{26}$Al. The $^{26}$Al/$^{27}$Al isotopic ratio can be obtained by measurements of the following three quantities: the $^{26}$Al total counts at the detector ($[^{26}Al^{3+}]_d$), the integrated $^{16}O^{2+}$ current at the monitor Faraday cup ($[^{16}O^{2+}]_m$), and the negative-ion current ratio at the ion source ($I_{26}/I_{26}$).[6] These quantities are expressed as follows:

$$[^{26}Al^{3+}]_d = [^{26}Al^-]_s \epsilon_1 \epsilon_2 , \quad (1)$$

$$[^{16}O^{2+}]_m = [^{10}B^{16}O^-]_s \epsilon_1' , \quad (2)$$

$$\frac{I_{26}}{I_{27}} = \frac{[^{10}B^{16}O^-]_s}{[^{27}Al^-]_s} , \quad (3)$$

where $I_{26}$, $I_{27}$ are the negative ion beam currents of $m/e=26$ and 27, $\epsilon_1$, $\epsilon_1'$ the transmission efficiency of accelerator for $^{26}Al^{3+}$ and $^{16}O^{2+}$, and $\epsilon_2$ the transmission efficiency from high energy analyzing magnet to detector. Subscripts $s$, $m$, and $d$ indicate ion source, monitor, and detector, respectively. Using Eqs. (1)–(3), the $^{26}$Al/$^{27}$Al isotopic ratio for a sample is expressed as follows:

$$\frac{[^{26}Al]_s}{[^{27}Al]_s} = \frac{[^{26}Al^{3+}]_d}{[^{16}O^{2+}]_m} \frac{\epsilon_1'}{\epsilon_1} \frac{1}{\epsilon_2} \frac{I_{26}}{I_{27}} . \quad (4)$$

This equation is valid for the measurement with 100% enriched $^{10}$B. So, in the case of 91.8% enriched $^{10}$B, $I_{27}$ must be replaced by $I_{27}-I_{26}$ (8.2/91.8). The transmission efficiencies $\epsilon_1$, $\epsilon_1'$, $\epsilon_2$ can be determined by the measurement of a standard sample of known $^{26}$Al/$^{27}$Al ratio ($9.12\times10^{-10}$). This standard sample was prepared by adding the $^{27}$Al carrier to the original $^{26}$Al standard sample of $AlCl_3$ in a HCl solution whose activity was certified to be 38.79 (dis/sec)/$g$ (±1.1%) in 1971 by the National Bureau of Standards. A blank sample produced from the unirradiated aluminum was also measured to check the background counts.

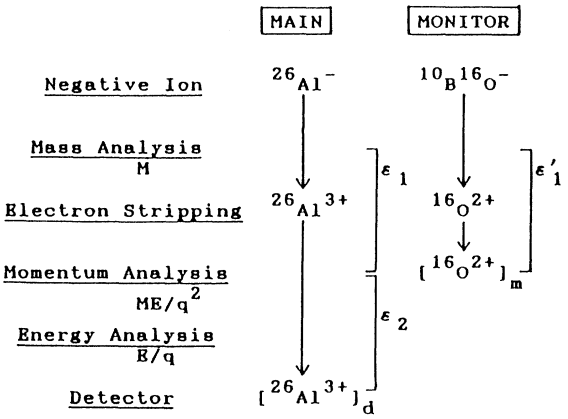


FIG. 2. Scheme of $^{26}$Al measurement by beam monitor with $^{10}B^{16}O$.

### C. Measurement procedure

Figure 3 shows the AMS system used in this work. The negative ions of $m/e=26$ ($^{26}Al^-$ and $^{10}B^{16}O^-$) and 27 ($^{27}Al^-$) were sputtered from a Cs sputtering ion source of HICONEX 834 (General Ionex Corp.) and accelerated by the extraction electrode. The $^{26}Al^-$ and $^{10}B^{16}O^-$ ions were selected by the negative ion analyzer magnet (90° deflection angle), injected into the tandem Van de Graaf accelerator, and converted to positive ions of $^{26}Al^{3+}$, $^{10}B^{3+}$, $^{16}O^{2+}$, etc., by the argon-gas stripper. These positive ions were accelerated and analyzed by the 90° analyzer magnet which was set for 10 MeV $^{26}Al^{3+}$. The $^{16}O^{2+}$ ions were deflected more strongly than $^{26}Al^{3+}$ ions, and the $^{16}O^{2+}$ current $[^{16}O^{2+}]_m$ in Eq. (2) was monitored at the Faraday cup (beam monitor) just behind the 90° analyzer magnet. Only $^{26}Al^{3+}$ ions were transported to the silicon detector of 300 mm$^2$ sensitive area (F-025-300-60 of ORTEC Co. Ltd.) through the magnetic switcher and the electrostatic deflector.

In order to obtain the parameter for the beam transport from the accelerator to the detector, $^{26}Mg^{3+}$ ions from enriched $^{26}Mg^{16}O^-$ were used to pass through the analyzer magnet which was set for 10 MeV $^{26}Al^{3+}$.

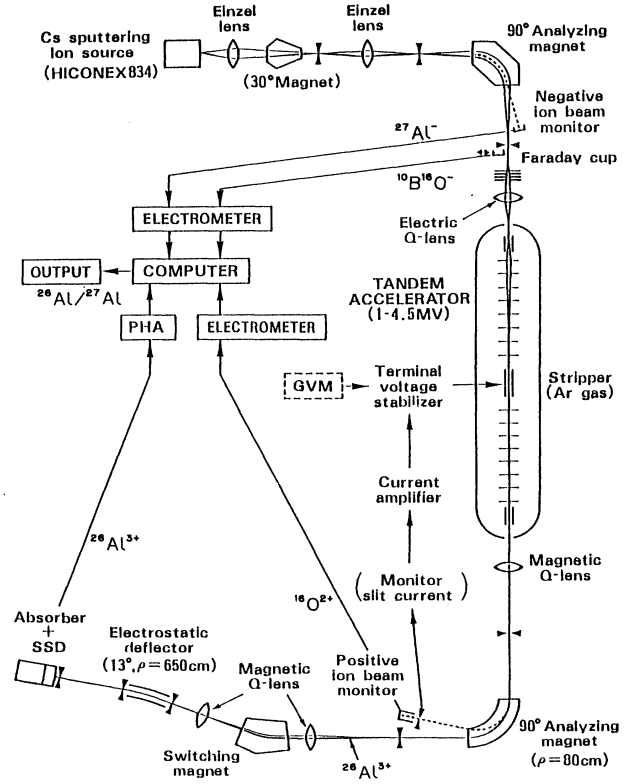


FIG. 3. Schematic diagram of accelerator mass spectrometry system at tandem Van de Graaf accelerator.

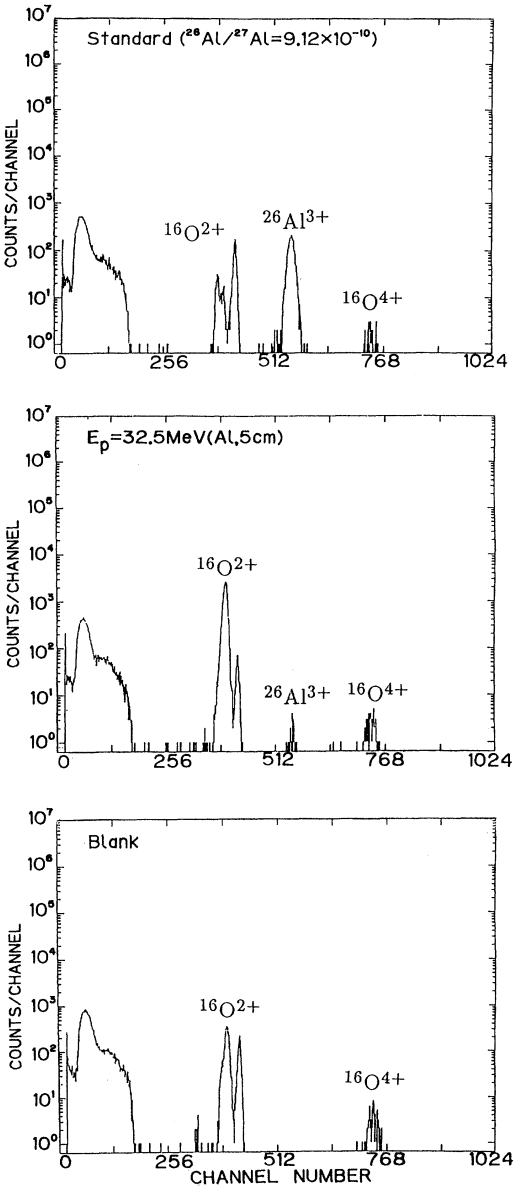


FIG. 4. Energy spectra measured with the silicon detector for irradiated sample, standard sample, and blank (unirradiated) sample.

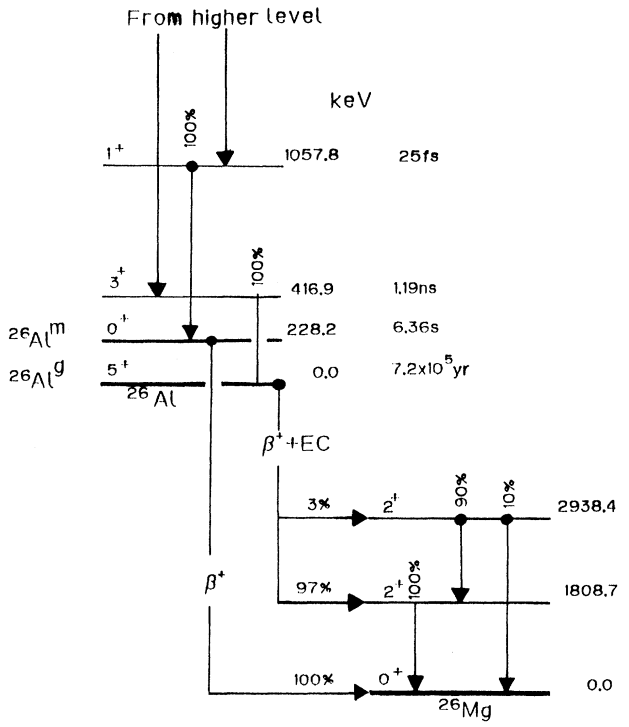


FIG. 5. Decay scheme of $^{26}Al$ cited from Ref. 14.

### D. Measured results

Figure 4 compares the energy spectra of Al samples irradiated at 5 cm from a Be target bombarded by 32.5 MeV protons with those of a standard sample and a blank (unirradiated aluminum) sample, which were measured by the silicon detector. Peaks other than $^{26}Al^{3+}$ were assigned to $^{16}O^{2+}$ (6.7 MeV) and $^{16}O^{4+}$ (13.3 MeV). A fairly large peak in the lowest-energy region of the spectra was not identified. From the blank-sample spectrum, the background level in the $^{26}Al$ region of the spectra was found to be less than $1\times10^{-13}$. The $^{26}Al$ measurements were repeated three to five times and each counting time was 1000 sec.

Table II lists the $^{26}Al/^{27}Al$ ratios obtained from Eq. (4) with statistical errors. These values are converted to the $^{26}Al$ activities and normalized to total proton currents per Coulomb injected to a Be target during irradiation.

TABLE II. Measured results of $^{26}Al/^{27}Al$ ratio and $^{27}Al(n,2n)^{26}Al^g$ cross sections.

| Proton energy (MeV) | 37.5 | 32.5 | 30.0 | 27.5 | 25.0 | 22.5 | 20.0 |
|---|---|---|---|---|---|---|---|
| Peak neutron energy (MeV) | 33.6 | 28.5 | 25.9 | 23.4 | 21.0 | 18.2 | 15.3 |
| $^{26}Al/^{27}Al$ | $1.203\times10^{-12}$ $\pm0.179$ | $2.599\times10^{-12}$ $\pm0.268$ | $3.466\times10^{-12}$ $\pm0.296$ | $3.761\times10^{-12}$ $\pm0.324$ | $1.160\times10^{-12}$ $\pm0.141$ | $1.429\times10^{-12}$ $\pm0.126$ | $8.136\times10^{-13}$ $\pm1.403$ |
| Cross section[a] (mb) | $4.196\times10^{1}$ $\pm1.260$ | $6.985\times10^{1}$ $\pm1.383$ | $8.203\times10^{1}$ $\pm1.034$ | $9.237\times10^{1}$ $\pm1.629$ | $8.987\times10^{1}$ $\pm1.159$ | $7.934\times10^{1}$ $\pm1.393$ | $3.515\times10^{1}$ $\pm1.116$ |

[a]Unfolded values by NEUPAC at peak neutron energy.

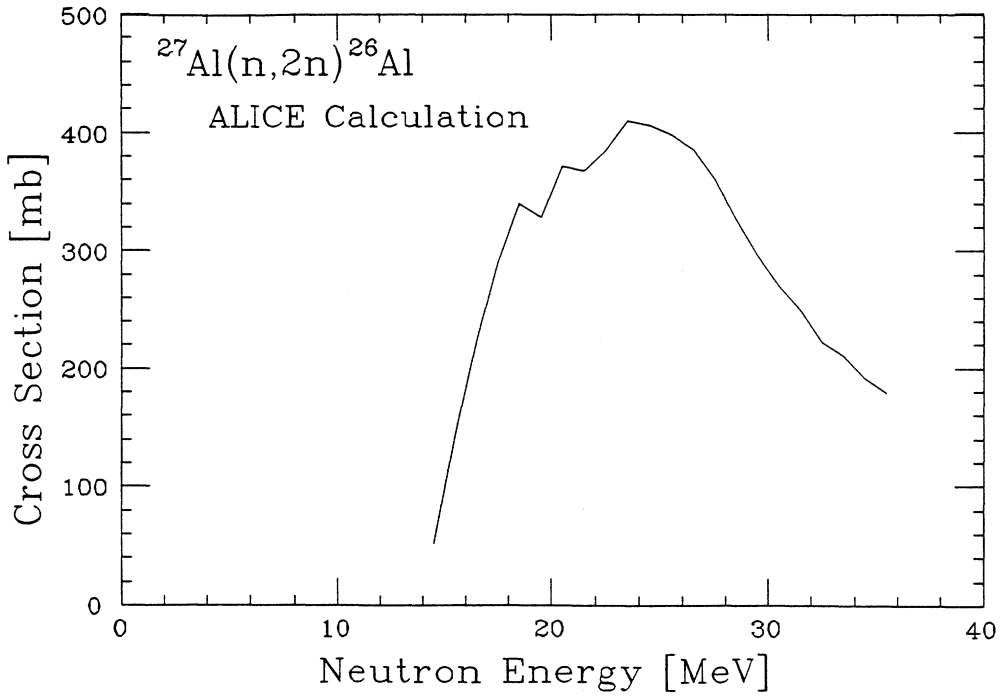


FIG. 6. $^{27}$Al$(n,2n)^{26}$Al$^{m+g}$ cross section, which is the sum of $^{27}$Al$(n,2n)^{26}$Al$^{g}$ producing the $5^+$ state of $^{26}$Al and $^{27}$Al$(n,2n)^{26}$Al$^{m}$ producing the $0^+$ isomeric state at 228 keV, calculated by the ALICE code.

## IV. DETERMINATION OF CROSS SECTION

The measured activity of $^{26}$Al, $A_i$ is related to

$$A_i = N \int_0^{E_p} \sigma(E)\phi_i(E)dE \ , \tag{5}$$

where $i$ is the $i$th experiment corresponding to each proton energy $E_p$, $N$ the number of $^{27}$Al nucleus in a sample, $\sigma(E)$ the $^{27}$Al$(n,2n)$ cross section, and $\phi_i(E)$ the neutron spectrum shown in Fig. 1. Since the neutron spectrum $\phi_i(E)$ is not purely monoenergetic but has a low-energy component, the $\sigma(E)$ value can be obtained by unfolding this integral equation. We finally obtained it with itera-

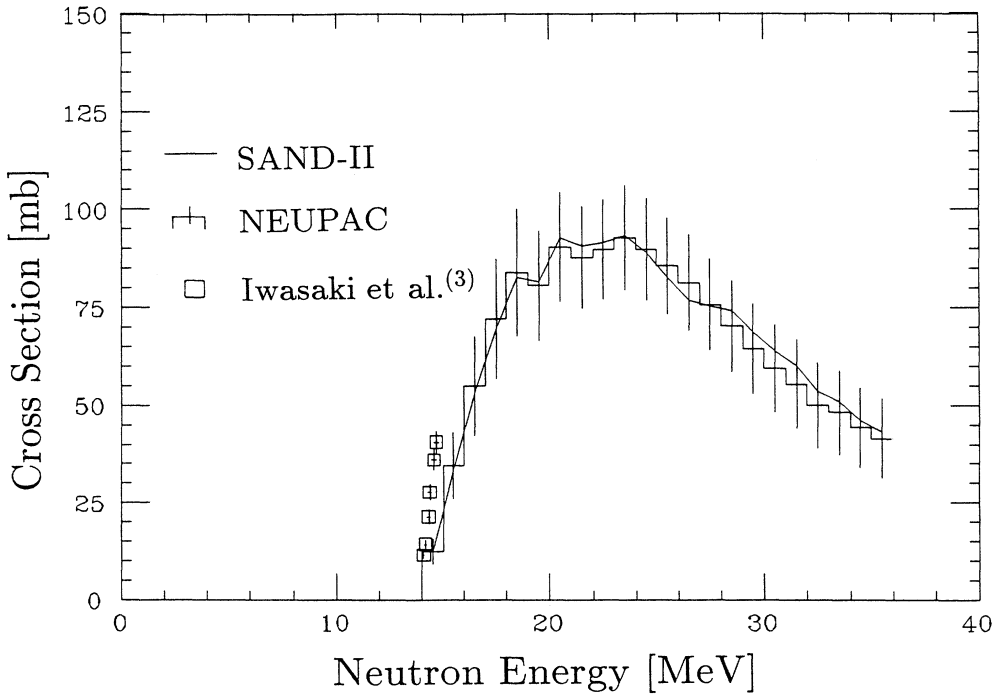


FIG. 7. Measured $^{27}$Al$(n,2n)^{26}$Al$^{g}$ cross-section data for neutron energies of 14 to 36 MeV.

tive perturbation method of the SAND-II code[10] and the $J1$-type unfolding method using the NEUPAC code.[11]

These codes required the initial guess value of $\sigma(E)$ for unfolding, which were calculated with the ALICE code[12] because of the lack of any experimental and calculated data of the $^{27}Al(n,2n)^{26}Al$ cross section. The ALICE code includes four reaction models of evaporation process and two reaction models of preequilibrium process. In this calculation, we selected the geometry-dependent hybrid model of preequilibrium process that gave the best fit in relative shape to the well-evaluated cross sections such as for $^{27}Al(n,\alpha)$ and $^{197}Au(n,2n)$ reactions.[13] The ALICE code only gives the total cross section of the $^{27}Al(n,2n)$ reaction, which is the sum of two partial cross sections of the $^{27}Al(n,2n)^{26}Al^g$ reaction producing the $5^+$ ground state of $^{26}Al$ and the $^{27}Al(n,2n)^{26}Al^m$ reaction producing the $0^+$ isomeric state at 228 keV (see Fig. 5). Figure 6 shows the $^{27}Al(n,2n)^{26}Al^{m+g}$ cross section calculated by ALICE.

The SAND-II code does not give unfolded errors, while, on the other hand, the NEUPAC code gives the errors propagated from errors of initial guess values, neutron spectrum, and activation rates of $^{26}Al$. The errors of neutron spectra are about 10% in the peak region and about 30–50 % in the low-energy region in Fig. 1, and the errors of $^{26}Al$ activation rates are 10–20 % in Table II. The relative errors of initial guess values by ALICE over the energy region are unknown; we assumed the errors of 30% in total for the NEUPAC unfolding.

Figure 7 shows the obtained results of $\sigma(E)$ in the neutron energy range of 14 to 36 MeV. Our results given by SAND-II and NEUPAC unfolding codes show very good agreement with each other. For near-threshold neutron energies, our experimental results are compared with other experimental data[1-3] in Fig. 8. Our data are lower than those other three results but closer to Sasaos's data.[2] Our results near threshold energy have rather poor accuracy due to the accumulation of unfolding errors and the larger experimental error of $^{26}Al$ activity for 20 MeV protons, as seen in Table II. The numerical data of $^{27}Al(n,2n)^{26}Al^g$ cross sections deduced by the NEUPAC unfolding are listed in Table II for the peak neutron energy corresponding to the incident proton energy. Our results of the $^{27}Al(n,2n)^{26}Al^g$ cross section are the first experimental data that have been obtained above 15 MeV.

The experimental data of $^{27}Al(n,2n)^{26}Al^m$ (half-life of 6.3 sec) cross section by Mani *et al.*[15] have a peak value of 150 mb at 20 MeV, which is 1.6 times larger than the 95 mb peak value at 20–24 MeV for $^{27}Al(n,2n)^{26}Al^g$. As described before, the ALICE code only gives the total cross section of the $^{27}Al(n,2n)^{26}Al^{m+g}$ reaction. The cross section calculated by ALICE shown in Fig. 6 has a maximum value of 400 mb around 24 MeV and this absolute value is about 1.6 times higher than the sum of our experimental value of 95 mb maximum at around 20 to 24 MeV for $^{27}Al(n,2n)^{26}Al^g$ and Manis's value of 150 mb around 20 MeV for $^{27}Al(n,2n)^{26}Al^m$.

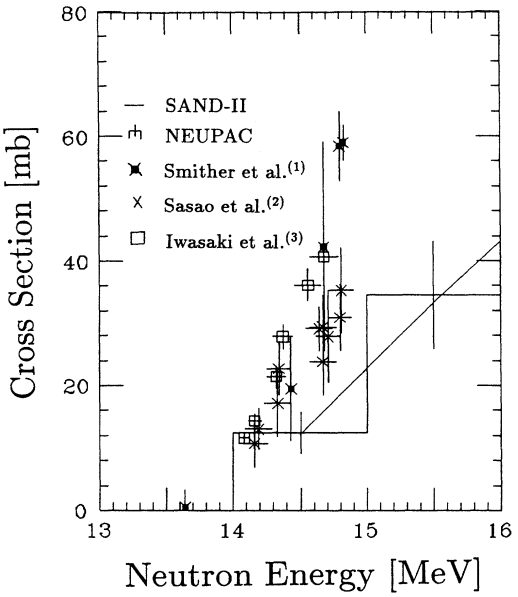


FIG. 8. Comparison of measured $^{27}Al(n,2n)^{26}Al^g$ cross-section data for near-threshold neutron energies.

## ACKNOWLEDGMENTS

The authors wish to thank H. Yamashita for his kind cooperation on the $^{26}Al$ measurement by the AMS system, and also the cyclotron machine group for their cyclotron operation. This work was financially supported by a Grant-in-Aid for Cooperative Research of the Japanese Ministry of Culture and Education.

[1] R. K. Smither and L. R. Greenwood, J. Nucl. Mater. **122&123**, 1071 (1984).

[2] M. Sasao, T. Hayashi, K. Taniguchi, A. Takahashi, and T. Iida, Phys. Rev. C **35**, 2327 (1987).

[3] S. Iwasaki, J. R. Dumais, and K. Sugiyama, *Proceedings of the International Conference on Nuclear Data for Science and Technology, Mito, 1988,* edited by S. Igarasi (Japan Atomic Energy Research Institute, Mito, 1988), p. 295.

[4] W. Henning, W. Kutschera, M. Paul, R. K. Smither, E. J. Stephenson and J. L. Yntema, Nucl. Instrum. Methods, **184**, 247 (1981).

[5] Y. Uwamino, T. Ohkubo, A. Torii, and T. Nakamura, Nucl. Instrum. Methods A **271**, 546 (1988).

[6] H. Nagai, T. Kobayashi, M. Honda, M. Imamura, K. Kobayashi, K. Yoshida and H. Yamashita, Nucl. Instrum. Methods B **29**, 266 (1987).

[7] K. Shin, Y. Uwamino, and T. Hyodo, Nucl. Technol. **53**, 78 (1981).

[8] Y. Uwamino, K. Shin, M. Fujii, and T. Nakamura, Nucl. Instrum. Methods **204**, 179 (1982).

[9] Y. Uwamino, H. Sugita, Y. Kondo, and T. Nakamura (to be submitted to Nucl. Sci. Eng.).

[10] W. N. McElroy, S. Berg, T. Crockett, and R. G. Hawkins, Air Force Weapons Laboratory Report No. AFWL-TR-67-41,

1967, Vols. I–IV.
[11]A. Sekiguchi, M. Nakazawa, and N. Ueda, Power Reactor and Nuclear Fuel Development Corporation Report No. PNC J260 85-01, 1985.
[12]M. Blann and J. Bisplingshoff, Lawrence Livermore National Laboratory Report No. UCID 19614, 1983.
[13]Y. Kondo, Master's thesis, Department of Nuclear Engineering, Tohoku University, 1989.
[14]Table of Isotopes, edited by C. M. Lederer and V. S. Shirley, 7th ed. (Wiley, New York, 1978), p. 48.
[15]G. S. Mani, G. J. McCallum, and A. T. G. Ferguson, Nucl. Phys. **19**, 535 (1960).